Classical dynamics of a family of billiards with analytic boundaries

1983 J. Phys. A: Math. Gen. 16 3971

(http://iopscience.iop.org/0305-4470/16/17/014)

J. Phys. A: Math. Gen. **16** (1983) 3971–3986. Printed in Great Britain

Classical dynamics of a family of billiards with analytic boundaries

Marko Robnik

Institut für Astrophysik, Universität Bonn, Auf dem Hügel 71, D-5300 Bonn, FRG

Received 6 May 1983

Abstract. The classical dynamics of a billiard which is a quadratic conformal image of the unit disc is investigated. We give the stability analysis of major periodic orbits, present the Poincaré maps, demonstrate the mixing properties by following the evolution of a small element in phase space, show the existence of homoclinic points, and calculate the Lyapunov exponent and the Kolmogorov entropy h. It turns out that the system becomes strongly chaotic (positive h) for sufficiently large deformations of the unit disc. The system shows a generic stochastic transition. The computations suggest that the system is mixing if the boundary is not convex.

1. Introduction

The work presented here is a numerical study of the classical dynamics of a certain family of billiards with analytic boundaries. I studied this billiard originally in order to analyse the statistical properties of its quantum mechanical energy spectrum, in particular the distribution of the level spacings. It became clear very soon that the classical dynamics of the system is rich enough to present a lot of phenomena of nonlinear dynamics. As the family parameter is varied, the system goes through a stochastic transition. The limiting cases are the integrable and a mixing system (most probably). We can thus observe the destruction of KAM-invariant tori, the arising of homoclinic points and the mixing properties. Moreover, since for a calculation of the orbits no integration is needed, we are able to determine the Kolmogorov entropy as a function of the parameter and thus observe its variation along with the stochastic transition. A global qualitative and quantitative knowledge of the classical dynamics is important for our understanding of the correspondence to the quantum mechanics of the system, which will be presented in a second paper of this series.

It is not the purpose of the present work to give any introduction or a brief review on chaotic behaviour in classical and quantum mechanics. Readers not familiar with the field may wish to consult the following reviews and the references therein: Berry (1983, 1978), Chirikov (1979), Helleman (1980), Zaslavsky (1981), Robnik (1983).

2. The definition of the family of billiards

Our billiard is shown in figure 1. It is the image (in the complex w plane) of the unit disc (in the z plane) under the quadratic conformal map $w = Az + Bz^2$. Its boundary

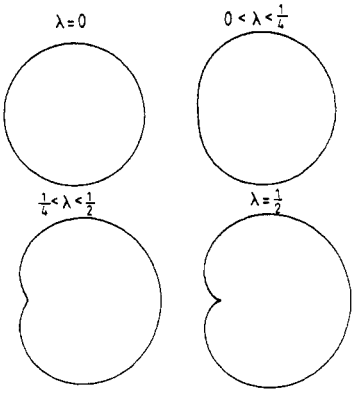

Figure 1. We show how the shape of the billiard changes as the parameter $\lambda = B/A$ varies.

is given by ($w =: u + iv$)

$$u = A\cos\varphi + B\cos 2\varphi, \qquad v = A\sin\varphi + B\sin 2\varphi, \tag{1}$$

where φ is the polar angle of the unit circle in the z plane. A non-parametric form of the equation (1) in rectangular coordinates u, v reads

$$(u^2+v^2-B^2)^2 = A^2(u^2+v^2) + 2BA^2u + B^2A^2. \tag{2}$$

We shall always denote $\lambda = B/A$. For $\lambda = 0$ we have a disc, for $0 < \lambda < \frac{1}{4}$ the billiard is convex, but at $\lambda = \frac{1}{4}$ the curvature of the boundary at $\varphi = \pi$ changes sign. For $\lambda = \frac{1}{2}$ the zero of the derivative coincides with the point $\varphi = \pi$, and a cusp occurs there.

We shall study the dynamics of a point particle moving freely in the interior and obeying the reflection law at the boundary. The parameter range of our family is $0 < \lambda < \frac{1}{2}$, so that the boundary is analytic everywhere. We assume a unit speed. It would be enough to study the system as a function of $\lambda = B/A$, with A equal to unity. However, for investigations of the quantum mechanical energy spectrum it is useful to have a family of billiards of constant area. The area of our billiard is equal to

$$\mathcal{A} = \pi(A^2 + 2B^2). \tag{3}$$

We introduce a curve of billiards of constant area, going through the point $A = 1$, $B = 0$. Thus $\mathcal{A} = \pi$. The family can be parametrised as

$$A = \cos p, \qquad B = (1/\sqrt{2})\sin p, \tag{4}$$

so that

$$p = \tan^{-1}(\lambda\sqrt{2}). \tag{5}$$

The parameter range is $0 < p < \tan^{-1}(1/\sqrt{2}) = 0.615\,4797\ldots$.

3. The orbits in configuration space

An orbit is uniquely determined by the initial position on the boundary, specified by the angle $\varphi \in (0, 2\pi)$, and by the initial direction, specified by the angle $\chi \in (-\pi/2, \pi/2)$ between the velocity vector and the inward normal to the boundary. The numerical

study of the orbits has been done on the CDC Cyber 172 computer with accuracy to 25 decimal places (double precision). The time evolution is determined if the map $\Phi:(\varphi_0, \chi_0) \to (\varphi_1, \chi_1)$ is known, where φ_1, χ_1 are the new collision point on the boundary and the reflection angle, respectively. The calculation of Φ involves finding zeros of a certain function, only.

In figure 2 we show a typical non-periodic orbit for several parameter values p. For small p a caustic is formed—an indication that invariant tori exist. At larger p the caustic shrinks and finally disappears, showing that the invariant tori are destroyed. For $p > 0.338$ the orbit seems to fill the entire billiard uniformly. As we shall see, this is a consequence of strong stochasticity.

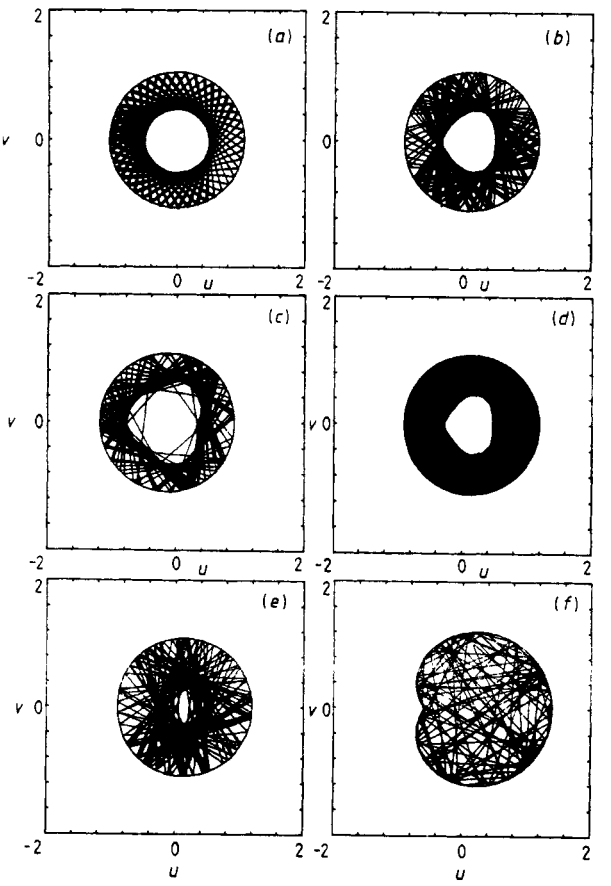

Figure 2. A non-periodic orbit with the initial conditions $\varphi = 0$, $\chi = 0.5$ at different values of (*a*) $p = 0.017\,319$ ($\lambda = 0.012\,248$), (*b*) $p = 0.172\,066$ ($\lambda = 0.122\,884$), (*c*) $p = 0.189\,014$ ($\lambda = 0.135\,268$), (*d*) same as in (*c*), (*e*) $p = 0.205\,890$ ($\lambda = 0.147\,679$), (*f*) $p = 0.514\,806$ ($\lambda = 0.4$). In all cases 100 collisions are shown, except in (*d*) where 1000 collisions are plotted. (The units on the coordinate axes are arbitrary.)

Periodic orbits exist at any p. Some of them are shown in figure 3. A periodic orbit of period n is specified by a finite sequence $(w_1, w_2, \ldots, w_n)$ of points on the boundary, where $w_{n+1} = w_1$, and $w_j = u_j + iv_j$ are complex numbers, $j = 1, 2 \ldots, n$. The

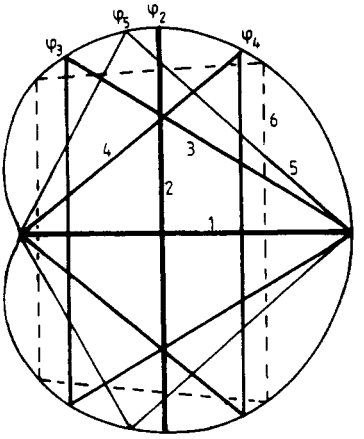

Figure 3. The major periodic orbits: period two (nos 1 and 2), period three (3 and 4) and period four (5 and 6). The upper collision point is uniquely determined by the parameter φ_j, $j = 2, 3, 4, 5$ (see equation (1)).

orbit is most easily calculated by using Fermat's principle: the length L of the orbit must be stationary, i.e. the first variation of

$$L = \sum_{j=1}^{n} |w_{j+1} - w_j| \tag{6}$$

must vanish.

The vertical period-two orbit clearly connects the maximum and the minimum. The position of the maximum at $\varphi = \varphi_2$ is given by

$$\cos \varphi_2 = (8\lambda)^{-1}[-1 + (1 + 32\lambda^2)^{1/2}]. \tag{7}$$

The upper collision points of orbits nos 3, 4 (period three) and no 5 (period four) are given by φ_3, φ_4, φ_5, respectively. From the stationarity of expressions (6) follows

$$\cos \varphi_3 + 2\lambda \cos 2\varphi_3 + \frac{\sqrt{2}}{2} \frac{\sin \varphi_3 + 2\lambda(1+\lambda) \sin 2\varphi_3}{[1+\lambda+\lambda^2 - \cos \varphi_3 - \lambda(1+\lambda) \cos 2\varphi_3]^{1/2}} = 0, \tag{8}$$

$$\cos \varphi_4 + 2\lambda \cos 2\varphi_4 - \frac{\sqrt{2}}{2} \frac{\sin \varphi_4 + 2\lambda(1-\lambda) \sin 2\varphi_4}{[1-\lambda+\lambda^2 + \cos \varphi_4 + \lambda(1-\lambda) \cos 2\varphi_4]^{1/2}} = 0, \tag{9}$$

$$\frac{\sin \varphi_5 + 2\lambda(1+\lambda) \sin 2\varphi_5}{[1+\lambda+\lambda^2 - \cos \varphi_5 - \lambda(1+\lambda) \cos 2\varphi_5]^{1/2}}$$

$$- \frac{\sin \varphi_5 + 2\lambda(1-\lambda) \sin 2\varphi_5}{[1-\lambda+\lambda^2 + \cos \varphi_5 + \lambda(1-\lambda) \cos 2\varphi_5]^{1/2}} = 0. \tag{10}$$

For all other periodic orbits, e.g. the broken period-four orbit in figure 3, the function L in (6) depends on more than one variable. Such orbits were not calculated.

Next we are interested in the neighbourhood of periodic orbits. The stability of period-two orbits is easy to study analytically. The linearisation of the map $\Phi \circ \Phi$ around the initial conditions of the periodic orbit (which is a fixed point of $\Phi \circ \Phi = \Phi^2$) leads to a unimodular ($\det = 1$) 2×2 matrix M, whose trace is equal to

$$\operatorname{Tr} M = 2[1 - 2l(1/r_1 + 1/r_2) + 2l^2/r_1 r_2], \tag{11}$$

where r_1, r_2 are the curvature radii of the boundary at the two collision points and l is the half-length of the closed path, i.e. l is the distance between the 'mirrors'. The eigenvalues μ of M are thus determined by

$$\mu^2 - \mu \operatorname{Tr} M + 1 = 0. \tag{12}$$

They are either complex conjugates on the unit circle (if $|\operatorname{Tr} M| < 2$) or real reciprocals (if $|\operatorname{Tr} M| > 2$).

3.1. The horizontal orbit (orbit no 1)

The dimensionless curvatures l/r_1, l/r_2 at the right and left point, respectively, are given by

$$\frac{l}{r_1} = 2\frac{1+4\lambda}{(1+2\lambda)^2}, \qquad \frac{l}{r_2} = 2\frac{1-4\lambda}{(1-2\lambda)^2}. \tag{13}$$

(Here we see that l/r_2 changes sign at $\lambda = B/A = \frac{1}{4}$.) Hence,

$$\operatorname{Tr} M = 2(1-40\lambda^2+16\lambda^4)/(1-4\lambda^2)^2, \tag{14}$$

which is plotted in figure 4. The horizontal orbit becomes unstable ($\operatorname{Tr} M = -2$) at $\lambda = (\sqrt{2}-1)/2 = 0.207\,106\,78\ldots$.

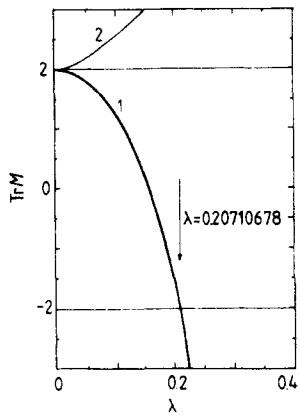

Figure 4. The result of the analytical stability analysis of the period-two orbits (see figure 3). We plot the trace of the matrix M, which is the linear part of Φ^2 near the periodic point. The arrow shows where the orbit 1 goes unstable and doubles.

3.2. The vertical orbit (orbit no 2)

Due to symmetry $l/r_1 = l/r_2$, and this is equal to

$$\frac{l}{r} = 2\frac{[3+(1+32\lambda^2)^{1/2}](1+32\lambda^2)^{1/2}}{1+(1+32\lambda^2)^{1/2}}. \tag{15}$$

It turns out that the trace is always greater than 2, as shown in figure 4. Thus the vertical period-two orbit is unstable for any λ.

It will be seen in § 4 that orbit no 1 is the most important, in the sense that it is surrounded by the largest stability island. Since $\operatorname{Tr} M = -2$ at the bifurcation point, the

eigenvalues are equal to minus one. So, it is a period doubling bifurcation. The subsequent series of period doubling bifurcations has been observed and the estimated limit is $\lambda^* \equiv 0.241$, or $p^* \equiv 0.402$. The doubled orbit no 1 is also seen by means of the Poincaré maps discussed in § 4. But it is interesting to see the doubled orbits in the configuration space (figure 5) as well.

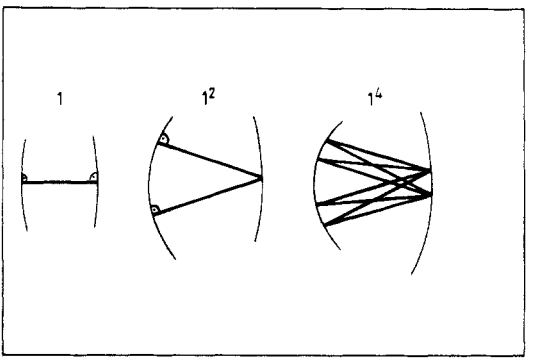

Figure 5. The first two bifurcations of the period doubling sequence of the orbit 1 in configuration space (schematically).

It is seen from figure 5 that the doubled orbit 1^2 can be easily specified in a geometric way: its angle φ_{1^2} determining the upper collision point (near $\varphi = \pi$) is given by the condition that the reflection angle χ vanishes there, which yields

$$\cos \varphi_{1^2} = -1/4\lambda(1+\lambda).$$

The orbit appears for the first time when the RHS is equal to minus one, which is precisely the condition for the instability of orbit 1, namely $\lambda = (\sqrt{2}-1)/2$. It is possible to calculate analytically the value of λ at which 1^2 bifurcates ($1^2 \to 1^4$) and becomes unstable (see table 1).

Table 1. Stability of the major periodic orbits.

Orbit no	Goes unstable at λ_{bif}
1	0.20710 67811 86547 52440 68444 $= (\sqrt{2}-1)/2$
2	0 (always unstable)
3	0 (always unstable)
4	0.1762
5	0.17602
6	0 (always unstable)
1^2	0.23751 88847 29279 19076 61218
1^∞	0.241 (extrapolared from 1 and 1^2)

The stability of orbits nos 3, 4, 5 can be studied analytically, but the expressions become too complicated. Their stability was investigated numerically. It turns out that orbit no 3 is always unstable, while orbit no 4 is found to be stable for $0 < p <$ 0.2442. Similarly, orbit no 5 of period four is stable in the interval $0 < p < 0.243\,97$, while orbit no 6 is unstable for all p. The stability analysis is summarised in table 1.

4. The Poincaré maps

A complete knowledge of a dynamical system can be reached only by exploring its phase space. Usually, the practical way of doing this is to introduce a surface of section (SOS) and to investigate the Poincaré map defined by the flow. For billiards the natural coordinates on SOS are the arc length parameter s of the boundary and the tangential velocity, i.e. the sine of the reflection angle, $\sin\chi$. They are canonically conjugate, which means that the Poincaré map is area preserving. In our case it is more convenient to take the parameter φ (the polar angle of the unit circle in the z plane) instead of s, because s is related to the coordinates u, v by an elliptic integral. Defined in this manner the map is not area preserving, but it preserves the topology of the phase portrait on SOS.

A series of Poincaré plots is shown in figure 6. At $p=0$ we have a circular disc and the phase portrait is dull (not shown): each horizontal line is an invariant torus. It consists of periodic points of period n if $\chi=(n-2)\pi/2n$. For a small value of p, such as in figure 6(a), the system is almost integrable. Most of the invariant curves still exist, although some of the rational tori are already destroyed, however. This is the case for period-two invariant curves. But two stable periodic points and two unstable periodic points survived the perturbation, as predicted by the Poincaré–Birkhoff theorem. They correspond to orbits nos 1 and 2, respectively. The stable four-cycles correspond to orbit no 5 of figure 3. The lower cycle describes a clockwise rotation, and the upper one a counterclockwise rotation. Between the stable periodic points there are unstable points of period four, and they correspond to the broken orbit of figure 3.

The invariant curve consisting of period-three points ($\chi=\pi/6$) is also broken, but for each of the two there is a stable and an unstable three-cycle which survived the perturbation of the disc. (The positions of the corresponding hyperbolic and elliptic periodic points are indicated, but no tori around them are shown.) We see that all low-resonance invariant curves are destroyed for small perturbations of the circular disc, as is permitted by the KAM theorem. Between the persisting invariant curves there may be regions of 'microscopic' stochastic motion. While confined between the irrational tori, the chaotic motion cannot be observed on the 'macroscopic' scale.

With increasing value of p still more invariant curves are successively destroyed and the chaotic motion in resonant gaps can eventually be observed on the 'macroscopic' scale (figure 6(b)). These stochastic regions develop near the separatrices connecting the unstable periodic points, as is clearly seen for period three, for instance.

An interesting question is: when does the last large-scale torus break up? (By large-scale invariant curve we mean a simple connected invariant curve existing for all $\varphi\in(0,2\pi)$. It thus separates the phase space (SOS) in two disjoint regions.) At the moment when this last large-scale torus is broken the particle can make excursions through the entire phase space, with the exception of small stability islands. This seems to happen quite abruptly at some p between $p=0.172$ (figure 6(b)) and $p=0.214$ (figure 6(c)). The two curves in figure 6(c) near $\sin\chi=\pm0.9$ are virtual invariant curves, because after $>10\,000$ collisions the particle diffuses into the chaotic region of SOS. This was observed in configuration space too. First, after a few hundred collisions a virtual caustic appears, but after roughly 10 000 the unoccupied part of the billiard is slowly filled. Hence this is a 'state' localised around a *virtual torus* only for finite, but nevertheless large, times. These virtually localised orbits are responsible for the fluctuations in the plot density in the chaotic region. The reason for the transient

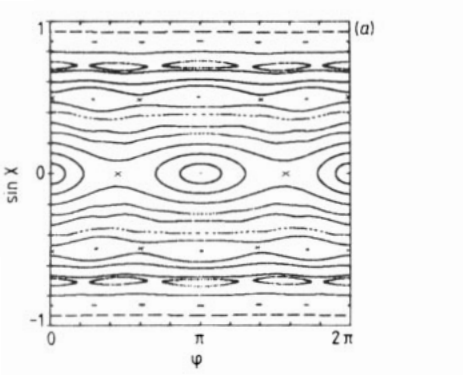

Figure 6. (*a*) The Poincaré surface of section at $p = 0.129\,4205$ ($\lambda = 0.092\,029$). The ordinate is the sine of the reflection angle, and the abscissa is the parameter determining the position of the collision point on the boundary (see equation (1)).

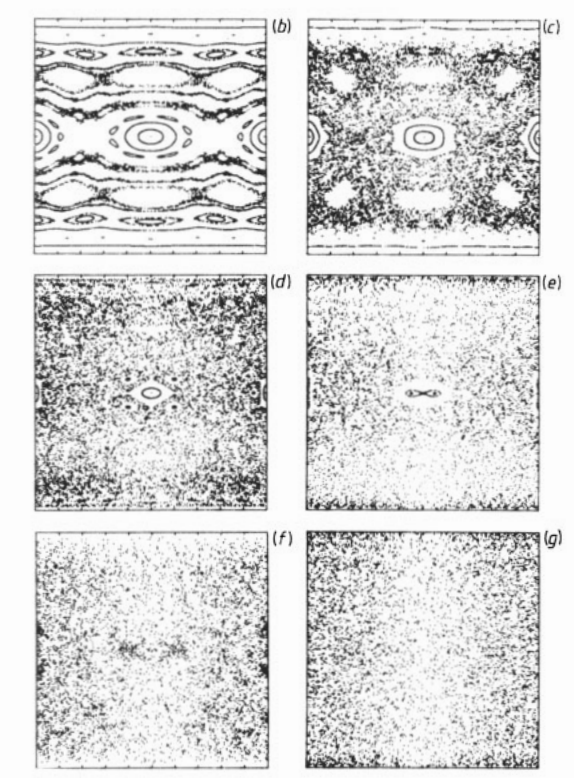

Figure 6. (*b*)–(*g*) The Poincaré surface of section at (*b*) $p = 0.172\,066$ ($\lambda = 0.122\,884$), (*c*) $p = 0.214\,299$ ($\lambda = 0.153\,895$) (*d*) $p = 0.256\,029$ ($\lambda = 0.185\,102$), (*e*) $p = 0.297\,173$ ($\lambda = 0.216\,545$), (*f*) $p = 0.337\,658$ ($\lambda = 0.248\,268$), (*g*) $p = 0.377\,420$ ($\lambda = 0.280\,314$). The scale on the coordinate axes is as in figure 6(*a*).

localisation is the slow diffusion between the remnants of a broken torus, which consist of chains of 'microscopic' stability islets. The diffusion is not quite smooth, but can be interrupted by abrupt and rapid spreading. This occurs, however, at large time

intervals, typically a few thousand collisions. The origin of such jumps is obviously the encounter of a hyperbolic orbit or its neighbourhood.

Such fluctuations implied by the slowness of the spreading of orbits are also observed in figure 6(*d*), where $p = 0.256\,0289$. (Note that the smooth variation of the density along the abscissa is due to the fact that our map is not area preserving. In other words, the invariant measure of the flow is proportional to the area element of our SOS times the derivative $ds/d\varphi$.) All large scale invariant curves have disappeared, and the size of the islets of stability decreases rapidly. The largest island surrounds the stable period-two orbit. In its vicinity there is a chain of smaller islands around a stable four-cycle.

In figure 6(*e*), the horizontal period-two orbit is already unstable, but in the neighbourhood there are stable periodic orbits of period four, which were born by the period doubling bifurcation of orbit no 1, and correspond to the doubled orbit shown in figure 5. This orbit goes unstable at $p = 0.324\,06\ldots$ ($\lambda = 0.237\,518\,88\ldots$). Having two values of the parameter p of the period doubling sequence of orbit no 1, we can use the well known universal behaviour for area preserving maps (Greene *et al* 1981) to predict the convergence limit $p^* = (\delta p_1 - p_0)/(\delta - 1) = 0.33$ ($\lambda^* = 0.241$) which is very near the point $p = 0.339\,837\ldots$ (perhaps coincident) at which the curvature changes sign ($\lambda = \frac{1}{4}$). (Here $\delta = 8.721\,097\,200\ldots$ is the universal rescaling parameter.) Otherwise the motion on the SOS is everywhere stochastic and becomes even more so at larger p such as shown in figure 6(*f*), where the fluctuations of the density are still visible, but disappear in a smooth sea of chaotic motion of figure 6(*g*).

5. The homoclinic points and the mixing property

In figure 7 we demonstrate the meaning of the mixing property of a dynamic system. We show how a small element Γ of figure 7(*a*) evolves in time (figures 7(*b*)–(*e*)). Its image under the evolution map Φ is shown for 1, 2, 3 and 4 collisions. The process is really very much like the mixing of milk in a cup of coffee. Remembering that the vertical sides of SOS should be identified, the reader can easily recognise a transformation shown schematically in figure 8.

The evolution of Γ in stable, integrable regions with invariant tori is in contrast to this behaviour. For example, at $p = 0.172\,066$, Γ lies completely within a stable island surrounding the periodic point of period two (see figure 6(*b*)). Therefore $\Phi^n(\Gamma)$ remains confined within tori forever and its form is hardly distorted even after 100 collisions as shown in figure 9.

An intermediate situation occurs if Γ lies partially in a stable island and partially in a stochastic region (figure 10). The central core remains trapped by tori, whereas its envelope is deformed into a filamentary structure and the filaments are pulled out and wind in a turbulent way to form 'hairs' of the core.

We now show the existence of the homoclinic points. To do this let us look more closely at the orbit no 1 of period two, the instability interval of which has been determined rigorously in § 3. In the Poincaré plot of figure 6(*e*) this orbit is already unstable and appears there as a pair of hyperbolic periodic points located at $\varphi = 0$ and $\varphi = \pi$ on the axis $\chi = 0$. Take that one sitting at $\varphi = \pi$. Its stable and unstable manifolds join smoothly, forming a separatrix. The question is when do they cross transversally? We claim that in figure 7(*c*) the manifolds do meet transversally. To see this observe that the element Γ is a neighbourhood of the hyperbolic point, which is a fixed point

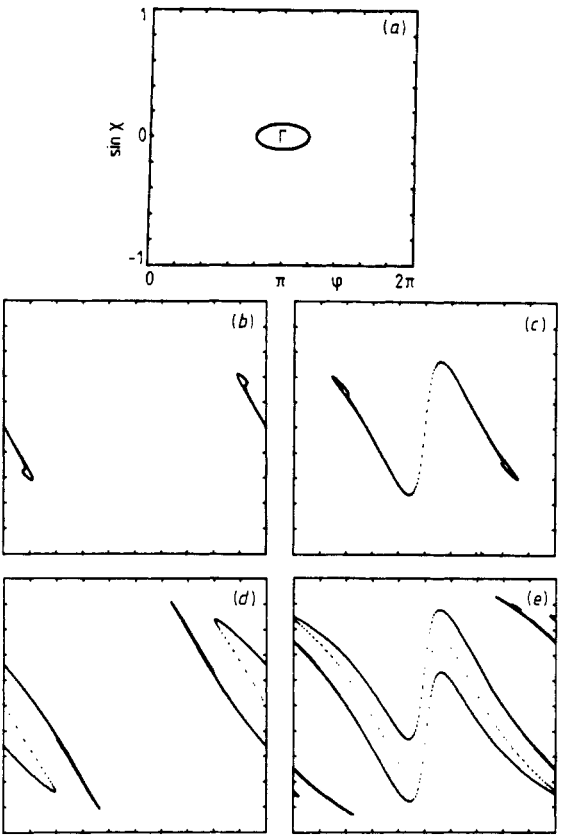

Figure 7. The mixing property of the billiard at $p = 0.514\,806$ ($\lambda = 0.4$). We show the evolution of the element Γ (a) in phase space after one (b), two (c), three (d) and four collisions (e). At the symmetry centre of Γ sits a hyperbolic periodic point of period two associated with orbit 1.

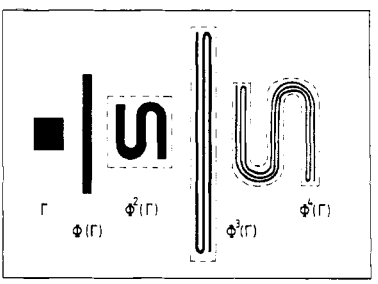

Figure 8. The 'kneading transformation' responsible for the mixing property shown in figure 7.

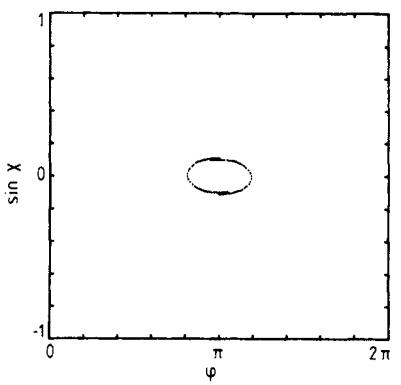

Figure 9. The form of the element Γ as plotted in figure 7(a) after 100 collisions at $p = 0.172\,066$ ($\lambda = 0.122\,884$). Here Γ lies in a stability island. (See the Poincaré plot in figure 6(b).)

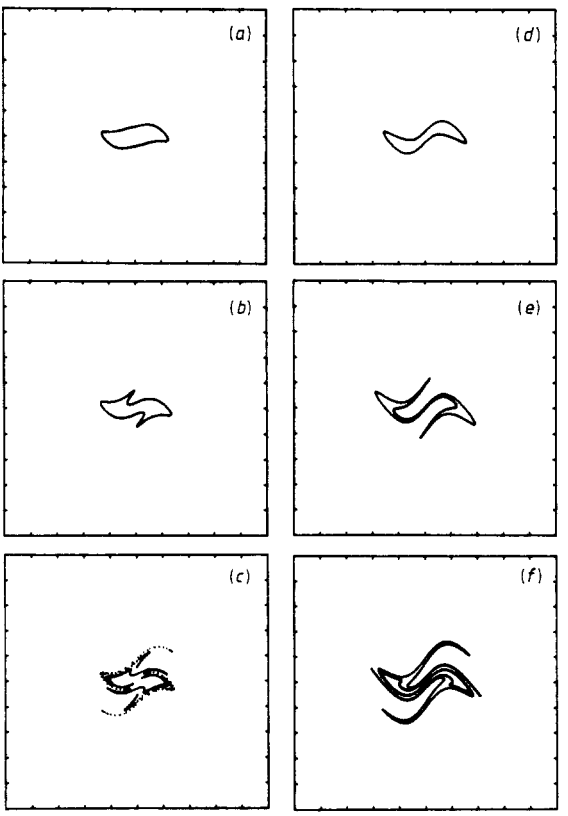

Figure 10. The evolution of the element Γ as plotted in figure 7(*a*) at $p = 0.305\,325$ ($\lambda = 0.222\,866$) for two (*a*), four (*b*), and ten collisions (*c*), and at $p = 0.337\,658$ ($\lambda = 0.248268$) for two (*d*), four (*e*) and six collisions (*f*).

of the second iterate Φ^2. It is clear that the thin ribbon $\Phi^2(\Gamma)$ follows the direction of the unstable manifold. Let us find the second iterate of the inverse map. As a little reflection shows, this is just the mirror image, i.e. $\Phi^{-2}(\Gamma)$ is obtained from $\Phi^2(\Gamma)$ by $\chi \to -\chi$. This ribbon is stretched along the stable manifold W^s, which crosses the unstable manifold W^u transversally at the point marked H in figure 11. In the small rectangle of the intersection $\Phi^2(\Gamma) \cap \Phi^{-2}(\Gamma)$ sits a homoclinic point (see the review by Guckenheimer (1979). Due to mirror symmetry it must lie exactly on the symmetry line $\chi = 0$. In this way we have constructed a map, defined by Φ^4 on the set $\Phi^{-2}(\Gamma)$, which is very much like Smale's horseshoe map. It is thus certainly non-integrable. We have actually good reasons to believe that the system is mixing (and thus ergodic) also globally (not only in a stochastic component) for sufficiently large p; most probably for $\lambda > \frac{1}{4}$, i.e. as soon as the boundary is not convex. In other words, at the moment when the boundary becomes non-convex the transversality occurs. Equivalently, one has to prove that one of the manifolds (and thus both) meets the symmetry line at skew angle for $\lambda > \frac{1}{4}$. The numerical evidence is strong in support of this, because homoclinic points exist already for $\lambda = 0.248\,268$ as can be inferred from figure 10(*e*). We note also that the convergence limit of the period doubling sequence coincides with this value of p within the observational accuracy $\Delta p = \pm 0.01$. A more detailed study of this interesting threshold is in progress.

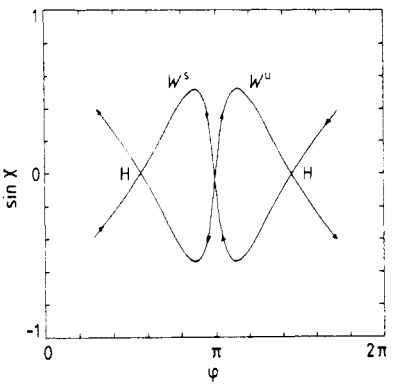

Figure 11. A homoclinic point H sits at the intersection of the stable manifold W^s and the unstable manifold W^u of the hyperbolic fixed point of Φ^2 (associated with orbit 1). W^s is revealed in figure 7(*c*), where $\Phi^2(\Gamma)$ follows its direction. W^u is the mirrored image of W^s with respect to the symmetry line $\chi = 0$. The inverse map $\Phi^{-2}(\Gamma)$ is stretched along W^u. Thus Φ^4 defines a map on the set $\Phi^{-2}(\Gamma)$ which is very similar to the horseshoe map. (Here p is the same as in figure 7.)

6. The Lyapunov exponent and the Kolmogorov entropy

A quantitative measure for the divergence of the flow is the Lyapunov exponent. Its definition for a quite general class of flows is based on the following facts (see Benettin and Strelcyn 1978). Take a tangent $\boldsymbol{e}$ at the point x in phase space M. Let Φ_x^t denote the flow carrying x along its orbit to the position $x(t)$ at time t, $\Phi_x^t : x \to x(t)$. If $\mathrm{d}\Phi_x^t$ is its derivative with respect to x (the tangent mapping), then the limit

$$\lim_{t\to\infty} t^{-1} \ln|\mathrm{d}\Phi_x^t(\boldsymbol{e})| = \Lambda(x, \boldsymbol{e}) \tag{16}$$

exists, and is finite for all $x \in M$, except for a set of Lebesque measure zero. (If M has a boundary, then those orbits which encounter the boundary for a finite t must be excluded too.) By $|\cdot|$ we denote the length (Euclidean metric) of a vector. It can be shown that: (i) $\Lambda(x, \boldsymbol{e})$ depends on x, on the direction of $\boldsymbol{e}$, but not on $|\boldsymbol{e}|$; (ii) it can assume at most three different values, the so-called Lyapunov characteristic numbers of the flow; (iii) for almost all $\boldsymbol{e}$ (in the sense of Lebesque) it is equal to the maximal characteristic number, $\Lambda_{\max}(x)$, which is always non-negative; (iv) $\Lambda_{\max}(x)$ is obviously constant along each orbit of the flow.

Hence the physical meaning: if two initial points are separated by a small distance $D_0(x)$, then as time goes on their separation D_t will (almost certainly) grow exponentially,

$$D_t(x) = D_0(x) \exp(\Lambda_{\max}(x)t). \tag{17}$$

Thus the Lyapunov exponent $\Lambda_{\max}(x)$ is the local measure for the exponential divergence of nearby orbits. Such exponential divergence is responsible for the 'coffee-and-milk' story of figure 7. After a short time the small element is evenly distributed in the phase space on some coarse scale. (Due to the Liouville theorem the microscopic volume is preserved.) It is useful to introduce such a coarsened scale. The coarsened volume Γ_t as a function of time increases exponentially,

$$\Gamma_t = \Gamma_0 \exp(\Lambda_{\max} t), \tag{18}$$

until is occupies the entire phase space and the evolution behaves as a diffusion process. In figure 7 this happens already after a few collisions.

In our case the time is the length of the orbit, because we assume unit speed. $\Lambda_{\max}(x)$, henceforth denoted just by $\Lambda(x)$, can be calculated numerically by the method explained by Benettin and Strelcyn (1978). The idea is to exploit the linearity of the tangent map $\mathrm{d}\Phi_x^t$. Starting with a segment $\boldsymbol{e}_i$ (of length $|\boldsymbol{e}_i| = 10^{-12}$, for instance), one calculates its length $\boldsymbol{e}_{i+1}$ after one collision, and rescales it to the original length. If $\beta_i = |\boldsymbol{e}_{i+1}|/|\boldsymbol{e}_i|$, then after n collisions the Lyapunov exponent is approximated by

$$\Lambda = \frac{1}{t} \sum_{i=0}^{n-1} \ln \beta_i. \tag{19}$$

In figure 12 we show a typical behaviour of Λ as it approaches its limiting value. The following facts have been observed numerically. (a) Small fluctuations (of order $<1\%$) were observed for quite large n, such as $n = 5000$. (b) The same limiting value was indeed found for all directions of the initial segment $\boldsymbol{e}$. (c) The limiting value of Λ is independent (within the fluctuations) of the length $|\boldsymbol{e}|$ over ten orders of magnitude ($10^{-16} < |\boldsymbol{e}| < 10^{-6}$). (d) Λ is found constant on a given stochastic component, which agrees with observations (and assumptions) by Benettin and Strelcyn.

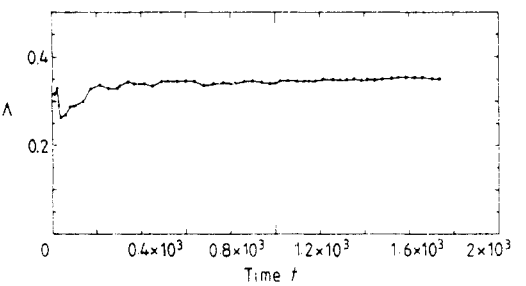

Figure 12. A typical run of the Lyapunov exponent as approximated by formula (19).

Whereas the Lyapunov exponent $\Lambda(x)$ measures the local divergence of orbits, one would like to define a quantity which does this globally for the entire phase space. Suppose that the phase space is a single stochastic component, containing a dense orbit. Then a global quantity characterising the divergence of the flow is given by the average over the phase space M,

$$h = \int_M \Lambda_{\max}(x)\, \mathrm{d}\mu, \tag{20}$$

and is called the Kolmogorov entropy. Here μ must be the normalised, invariant measure of the flow; for Hamilton systems this is the Liouville measure. Since M contains a dense orbit, such a definition is useful: h tells us what the mean divergence of orbits is. If M is the union of several invariant sets, for example if M consists of several stochastic components and stability islands, then the definition (20) is still useful. Because $\Lambda = 0$ in stability islands, whereas $\Lambda > 0$ on stochastic components, h measures the sum of two effects: the growth of size of the stochastic components, and

the increase of the value of Λ on them, when a system goes through a stochastic transition, such as shown in figure 6. The Kolmogorov entropy is thus a natural quantity to describe a stochastic transition.

To calculate h for a Hamilton system is a very hard problem generally. Firstly, $\Lambda(x)$ must be calculated on a sufficiently dense grid in phase space. Secondly, to calculate $\Lambda(x)$ at the grid point x one has to follow a pair of orbits for a sufficiently long time. Therefore, to calculate h for a smooth system like a hydrogen atom in a strong magnetic field (Robnik 1981, 1982) is impossible, because the numerical integration of orbits is too expensive. There are very few systems to date for which h has been calculated, notably the generalised stadion considered by Benettin and Strelcyn. Even for billiards, where no integration is necessary, the calculation of h is quite computer-time consuming. In our case we have taken a grid of 10×10 points in the quadrant $(\varphi, \sin\chi)\in(0, 2\pi)\times(0, 1)$. (Of course, in calculating the phase average (20) the true invariant measure was used.) At each grid point a pair of orbits was followed for 1000 collisions and $\Lambda(x)$ was calculated. Thus for a particular value of the parameter p one has to calculate 2×10^5 collisions. This has been done for 35 different values of p in order to obtain the graph of the Kolmogorov entropy $h(p)$ as a function of the family parameter p (figure 13). Altogether 7×10^6 collisions were calculated and the total computer time (CDC Cyber 172) used to plot the graph of figure 13 is about 30 hours. These facts demonstrate the importance and necessity of simple systems. In table 2 we list the values $h(p)$.

Figure 13 is believed to be typical for a system with a stochastic transition. We have marked the positions at which important bifurcations of periodic orbits occur.

An interesting and important question is whether the dependence of h on a parameter of the flow has some general universal properties. To decide this it is first

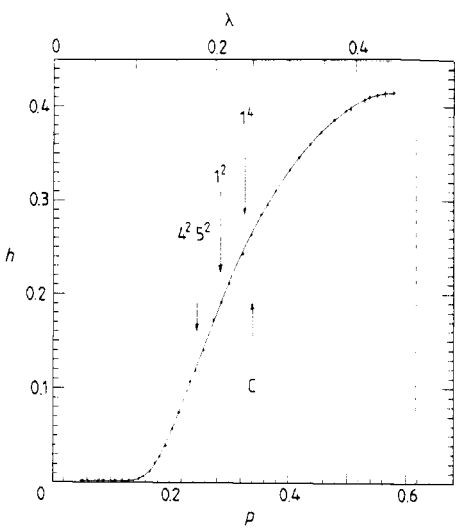

Figure 13. The Kolmogorov entropy h as a function of the parameter p. The area of the billiard is held constant and equal to $\mathscr{A}=\pi$. The speed of the particle is unity. At the same p but different speed v_1 and area $\mathscr{A}_1$ the entropy is equal to $h_1 = v_1 h(p)(\mathscr{A}/\mathscr{A}_1)^{1/2}$. The arrows indicate the positions of the most important bifurcations at which some of the major orbits go unstable. At the point marked C the billiard becomes non-convex. The thickness of dots corresponds to the error bars, except at the plateau of the maximum where they are larger (because of some numerical problems).

Table 2. The Kolmogorov entropy h as a function of the parameter p (or λ) at unit speed and area of the billiard $\mathcal{A} = \pi$.

p	$\lambda = B/A$	h	p	$\lambda = B/A$	h
0.052	0.037	0.001	0.322	0.236	0.243
0.086	0.061	0.002	0.337	0.248	0.264
0.104	0.074	0.002	0.354	0.261	0.285
0.129	0.092	0.003	0.364	0.269	0.296
0.146	0.104	0.004	0.377	0.280	0.312
0.156	0.111	0.007	0.401	0.300	0.333
0.164	0.117	0.012	0.417	0.313	0.346
0.172	0.123	0.022	0.437	0.330	0.361
0.180	0.129	0.028	0.455	0.346	0.373
0.193	0.138	0.039	0.477	0.365	0.386
0.202	0.145	0.058	0.492	0.379	0.396
0.214	0.154	0.075	0.506	0.392	0.398
0.231	0.166	0.101	0.529	0.413	0.409
0.243	0.175	0.118	0.536	0.420	0.411
0.256	0.185	0.140	0.550	0.433	0.413
0.276	0.200	0.173	0.564	0.447	0.416
0.286	0.208	0.191	0.578	0.461	0.416
0.298	0.217	0.211			

necessary to define some universal parameter for systems with a stochastic transition. Perhaps such a parameter is provided by the mean curvature of the associated geodesic flow, or by the relative invariant measure of the stochastic components. Another possibility is to look how $h(p)$ varies with p near the convergence limit p^* of the period doubling sequence for the most stable periodic orbits. As shown in figure 13, this limit goes along with the occurrence of homoclinic points and with the change of the curvature of the boundary. Interestingly, at the point of this triple coincidence the function $h(p)$ assumes roughly half of its maximal value and has the largest slope there.

7. Discussion and conclusion

In summary, we have demonstrated by numerical methods that our billiard with analytic boundaries is a generic system. As the family parameter p increases, the system is at first an almost integrable system with KAM-invariant tori which survived the perturbation of the circular disc, and later becomes a strongly chaotic system. Indeed, the described embedding of a horseshoe map near the homoclinic point and the large value of the Kolmogorov entropy, and the fact that no proper stochastic subcomponents are detected for $\lambda > \frac{1}{4}$, suggest the conjecture that the system is mixing (most probably on the parameter interval on which the boundary of the billiard is no longer convex). If the boundary is convex—in our case for $\lambda \in (0, \frac{1}{4})$—and smooth ($C^{553}$), then a general theorem by Lazutkin (1973) predicts the existence of caustics and invariant tori. Mather (1982) has recently supplemented Lazutkin's results: if the boundary is C^2 and if its curvature vanishes at least at one point, then there exist trajectories which come arbitrarily close to being positively tangent to the boundary and also come arbitrarily close to being negatively tangent to the boundary. This implies that caustics

and invariant tori cannot exist near the boundary as soon as the curvature vanishes at some point. Since the boundary of our billiard is analytic, both results, Lazutkin's and Mather's, apply and agree with numerical experiments.

Because the system is simple it has been possible to calculate the Kolmogorov entropy with relatively high precision. This is important for the study of the stochastic transition in classical systems, and for the verification of various predictions of the semiclassical theories on the statistical properties of energy spectra (Zaslavsky 1979, 1981, Robnik and Zaslavsky 1983). This will be studied in the next paper of this series.

Other questions concerning classical dynamics which seem worth pursuing further are the numerical study of the period doubling bifurcations, the determination of the sequence in which the large-scale tori are destroyed, the theoretical prediction for the location of existing but distorted KAM-tori, a study of ergodic properties—in particular a proof of the mixing property. In addition to this asymptotic behaviour it would be interesting to study the transient phenomena of long lived localisation of orbits near a virtual torus, as described in § 4.

Acknowledgments

I wish to thank George M Zaslavsky for a valuable communication. Sincere thanks are due Jean-Marie Strelcyn for important critical remarks. This work was supported by the Deutsche Forschungsgemeinschaft.

References

Bennettin G and Strelcyn J-M 1978 *Phys. Rev.* A **17** 773
Berry M V 1978 in *AIP Conf. Proc.* No 46, ed S Jorna (New York: AIP)
—— 1983 in *Proc. July 1981 'Les Houches' Summer School on Chaotic Behaviour of Deterministic Systems* ed R H G Helleman and G Iooss (Amsterdam: North-Holland)
Chirikov B V 1979 *Phys. Rep.* **52** 263
Greene J M, MacKay R S, Vivaldi F and Feigenbaum M J 1981 *Physica* **3D** 468
Guckenheimer J 1979 *Lectures in Applied Mathematics* vol 17, pp 187–253
Helleman R H G 1980 in *Fundamental Problems in Statistical Mechanics* vol 5, ed E G D Cohen (Amsterdam: North-Holland) pp 165–233
Lazutkin V F 1973 *Math. Izv. USSR* 186–216
Mather J N 1982 *Ergodic Theory and Dynamical Systems* **2** 3–4
Robnik M 1981 *J. Phys. A: Math. Gen.* **14** 3195
—— 1982 *J. Physique Coll.* **43** C2-45
—— 1983 in *Proc. August 1982 NATO–ASI Summer School on Photophysics and Photochemistry in the Vacuum UV* ed S McGlynn and G Findley
Robnik M and Zaslavsky G M 1983 *Phys. Rev. Lett.* (to be submitted)
Zaslavsky G M 1979 *Sov. Phys. Usp.* **22** 788
—— 1981 *Phys. Rep.* **80** 158–250